minerals

MDPI

Article

Coupled Effects of Time and Temperature on the Rheological and Pipe Flow Properties of Cemented Paste Backfill

Bo Liu [1], Yaoping Zhang [1,*], Xionggang Zou [1], Chaomei Zhang [1] and Yingjie Chang [2,*]

[1] College of Resources and Building Engineering, Gannan University of Science and Technology, Ganzhou 341000, China
[2] School of Civil and Resources Engineering, University of Science and Technology Beijing, Beijing 100083, China
* Correspondence: b20190033@xs.ustb.edu.cn (Y.Z.); d202210046@xs.ustb.edu.cn (Y.C.); Tel.: +86-13576786644 (Y.Z.)

Abstract: As mineral resources at shallow depths become increasingly depleted, the development of these resources is progressively shifting to greater depths. This transition presents challenges for the pipeline transport of cement paste backfill (CPB), particularly in terms of long-distance transport and elevated temperatures. To investigate this phenomenon, we conducted rheological tests, developed a resistance model that accounts for both time and temperature, and performed numerical simulations. The results show that the rheological parameters of CPB exhibit a gradual decline as the flow progresses. Specifically, at 20 °C, the plastic viscosity of CPB decreases by 1.6 Pa·s, and the yield stress decreases by 48.15 Pa; at 30 °C, the plastic viscosity decreases by 1.3 Pa·s, and the yield stress decreases by 18.69 Pa; at 40 °C, the plastic viscosity decreases by 0.84 Pa·s, and the yield stress decreases by 12.55 Pa; and at 50 °C, the plastic viscosity decreases by 0.58 Pa·s, with the yield stress decreasing by 12.53 Pa. Furthermore, the influence of shear time on the rheological properties of CPB diminishes as temperature increases within the range of 20 °C to 50 °C. These results offer significant insights for optimizing the pipeline transport of CPB in mining operations. These findings provide valuable guidance for pipeline transport of CPB in mining operations.

Keywords: cemented paste backfill; time-dependent rheological behavior; rheological properties; pipeline transportation

check for updates

Citation: Liu, B.; Zhang, Y.; Zou, X.; Zhang, C.; Chang, Y. Coupled Effects of Time and Temperature on the Rheological and Pipe Flow Properties of Cemented Paste Backfill. *Minerals* **2024**, *14*, 1221. https://doi.org/10.3390/min14121221

Academic Editor: Abbas Taheri

Received: 28 October 2024
Revised: 23 November 2024
Accepted: 28 November 2024
Published: 29 November 2024

Copyright: © 2024 by the authors. Licensee MDPI, Basel, Switzerland. This article is an open access article distributed under the terms and conditions of the Creative Commons Attribution (CC BY) license (https://creativecommons.org/licenses/by/4.0/).

1. Introduction

The extraction of mineral resources in the mining process often results in the generation of substantial waste rock and tailings, posing environmental risks [1,2]. In response, fill mining has emerged as an environmentally friendly method, offering advantages such as safety, high efficiency, and environmental protection, and it is widely adopted by major mining enterprises [3–5]. CPB represents a suspended system comprising cement, tailings, and water. With the continuous advancement of mining technology, CPB has evolved into a high-concentration paste with characteristics including non-stratification, non-segregation, non-bleeding, and high mechanical strength [6,7]. As a non-Newtonian fluid, CPB exhibits intricate rheological properties [6,8]. During its transportation through pipelines to the goaf, CPB encounters challenges such as pipeline blockage, explosions, and wear [9]. Consequently, experts and scholars have delved into researching the rheology of CPB.

The mining process typically generates significant amounts of waste rock and tailings, which present environmental risks [1,2]. Filling mining has emerged as an environmentally friendly method, providing advantages such as safety, high efficiency, and environmental protection, and it is widely adopted by major mining enterprises [3–5]. CPB constitutes a suspended system that includes cement, tailings, and water. As mining technology advances, CPB has developed into a high-concentration paste characterized by non-stratification, non-segregation, non-bleeding, and high mechanical strength [6,7]. CPB,

classified as a non-Newtonian fluid, demonstrates complex rheological characteristics [6,8]. During its transportation through pipelines to the goaf, CPB encounters challenges such as pipeline blockage, explosions, and wear [9]. Consequently, experts and scholars have delved into researching the rheology of CPB.

Rheological experiments indicate that the properties of CPB are affected by several factors, such as solid content, temperature, and material characteristics [10–12]. Zhao observed that an increase in water content results in a reduction of the yield stress of CPB [13]. Haruna observed that increasing the curing temperature and the content of water-reducing agents resulted in elevated yield stress and viscosity of CPB [14]. Cao found that an increase in solid content resulted in increased viscosity of CPB [15]. Xu's findings indicated that incorporating silica fume enhanced the yield stress of CPB while reducing its viscosity; conversely, flocculants negatively affected the rheological properties of CPB [16,17]. Zhou indicated that finer tailings led to diminished rheological properties of CPB [18]. Mineral resource development presents challenges for mine filling due to increased distances and higher temperatures. CPB exhibits non-Newtonian characteristics, specifically shear-thinning properties [19,20]. Following shearing, the internal floc network structure of CPB is compromised, leading to alterations in its rheological properties [21]. The thixotropic mechanism of CPB is depicted in Figure 1. When the polymer experiences shear, its structure is disrupted, leading to a reduction in viscosity. Upon cessation of shear, the structure gradually recovers over time. Due to the absence of a thixotropic recovery process in pipeline transport, this phenomenon is characterized as time-dependent rheological behavior.

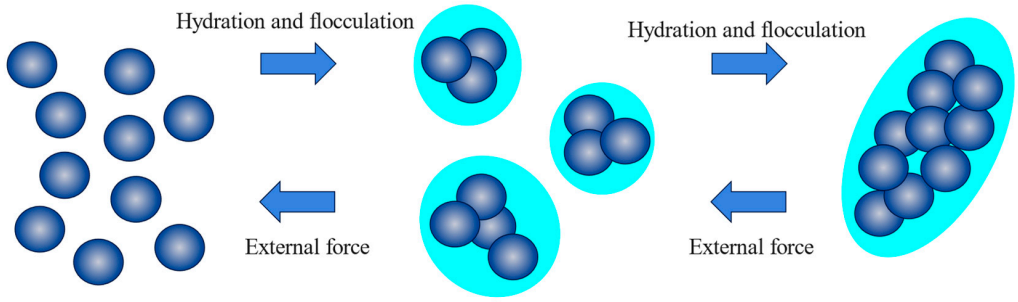


Figure 1. Schematic diagram of thixotropic mechanism.

Common models for calculating pipeline resistance in CPB include the Bingham model and the Herschel–Buckley (H-B) model [22,23]. These models, however, consider CPB as a time-independent fluid, neglecting the influence of shearing time on its rheological properties. The rheological properties of CPB change over time during pipeline transportation, resulting in inaccuracies in the calculations of transportation resistance.

To comprehensively characterize the rheological properties of CPB, a number of experts and scholars have devised innovative rheological models. Wu established a CPB rheological model considering cement hydration and temperature [24]. Liu developed a CPB rheological parameter prediction model using the backpropagation (BP) neural network [25]. Mewis elucidated thixotropy based on viscoelasticity theory, systematically classifying and evaluating existing thixotropic suspension rheological models [26]. Liu examined the thixotropic mechanisms of hydrostatic pressure drop in a Portland cement slurry [27]. Mendes proposed a novel numerical model to simulate the thixotropic behavior of viscoplastic fluids [28].

Given the susceptibility of pipeline transportation to external conditions and the inherent complexity of monitoring CPB pipeline flows, computational fluid dynamics (CFD) has emerged as a pivotal trend in pipeline transportation research. Kaushal [29] used the FLUENT software to numerically simulate the flow of monodisperse fine particles and high-concentration pipeline slurry by using the mixture two-phase model and the Euler two-phase model. Liu [30] conducted a numerical simulation of CPB pipeline transportation

that incorporated hydration effects. While existing studies have delved into the rheological properties and tube flow characteristics of CPB, few have explored the combined influences of time and temperature on these properties and tube flow characteristics. Consequently, there is a need to research the coupling effect of time and temperature on the rheological properties and pipe flow characteristics of CPB.

This study aims to evaluate the combined effects of time and temperature on the rheological properties and pipe flow characteristics of CPB. This study investigates the time-dependent rheological properties of CPB and formulates a computational model for pipe resistance that incorporates both time and temperature factors. Using numerical simulation software, we examine the pipe flow characteristics of CPB at different temperatures. This research's findings are significant for promoting the clean, efficient, and secure utilization of deep underground resources.

2. Materials and Methods

2.1. Materials

CPB was formulated by blending tap water with unclassified tailings (i.e., all particle sizes) sourced from Gaoguanying Iron Mine in Tangshan City, Hebei Province, China, P.O 42.5 Portland cement in accordance with the China Common Portland Cement Standard. The tailings' particle size distribution was assessed using a laser-diffraction particle size analyzer (Malvern, Worcestershire, UK), as illustrated in Figure 2. The key particle size parameters of unclassified tailings were as follows: d(10) = 1.82 μm, d(30) = 5.23 μm, d(50) = 10.51 μm, d(90) = 30.22 μm. The chemical composition of the tailings is presented in Table 1.

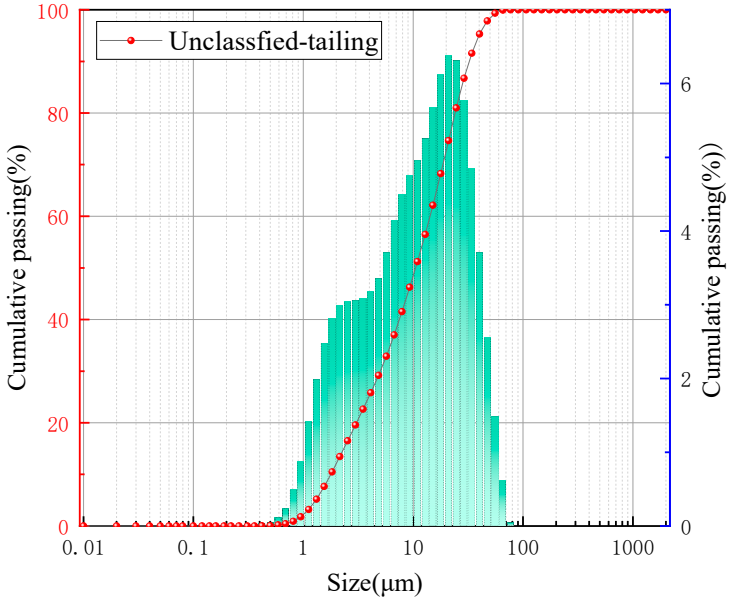


Figure 2. Particle size distribution.

Table 1. Chemical composition of tailings.

Chemical Composition	TFe	SiO_2	CaO	MgO	Al_2O_3	S	P	Other
Content (%)	6.00	67.58	4.04	5.60	7.30	0.21	0.16	9.11

2.2. Sample Preparation

The experimental design establishes the solid content of CPB at 66% by weight, with a cement-to-tailings ratio of 1:4. In the preliminary exploration experiments, this ratio exhibited characteristics typical of paste slurry, specifically a slump ranging from 15 to 25 cm, segregation of less than 2 cm, and a bleeding rate between 1.5% and 5% [31].

The combination of cement, unclassified tailings, and tap water was stirred at a constant temperature for 3 min to yield CPB.

2.3. Experiment Method

2.3.1. Rheological Test

The rheological tests for CPB were conducted using the HAAKES rheometer, as illustrated in Figure 3, equipped with a temperature control device. The rheometer features a four-bladed paddle rotor of type FL22 4B/SS-01170440. The test started with a 20 s pre-shear at a shear rate of 100 s^{-1}, followed by a 20 s resting period to ensure the consistency of the initial structure of the CPB. The controlled shear rate (CR) method was employed for the rheological tests [26], which comprised two parts: the shear rate ramp loading test (see Table 2) and the shear rate constant loading test (refer to Table 3). The tests were conducted at temperatures of 20 °C, 30 °C, 40 °C, and 50 °C.

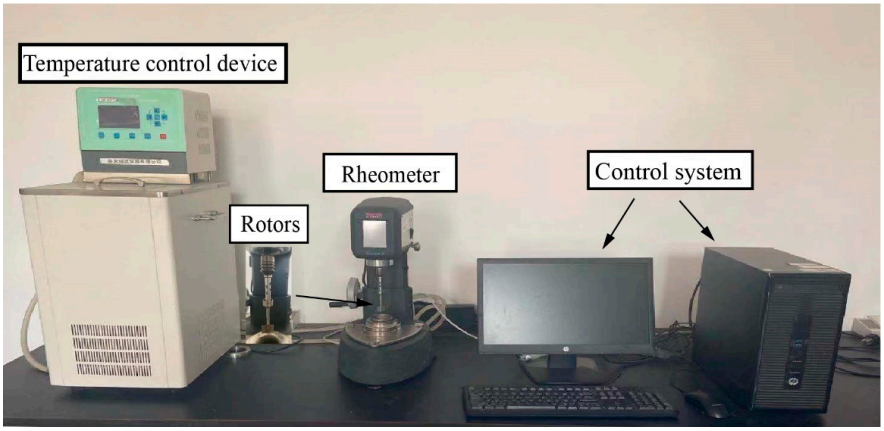


Figure 3. Test instrument.

Table 2. Shear rate ramp loading test procedure.

Sample ID	Shear Rate/s^{-1}	Temperature/°C	Shear Time/s
R-20	0–100	20	100
R-30	0–100	30	
R-40	0–100	40	
R-50	0–100	50	

Table 3. Shear rate constant loading test procedure.

Group ID	Sample ID	Shear Rate/s^{-1}	Temperature/°C	Shear Time/s
C-20	C-20-30	30	20	1000
	C-20-60	60		
	C-20-90	90		
	C-20-120	120		
C-30	C-30-30	30	30	
	C-30-60	60		
	C-30-90	90		
	C-30-120	120		
C-40	C-40-30	30	40	
	C-40-60	60		
	C-40-90	90		
	C-40-120	120		
C-50	C-50-30	30	50	
	C-50-60	60		
	C-50-90	90		
	C-50-120	120		

2.3.2. Numerical Simulation of CPB Pipeline Transportation

To characterize the time-dependent rheological behavior of CPB during pipeline transportation, we formulated a resistance equation that incorporates time-dependent rheological behavior (Equation (7)). This equation was then integrated into the numerical simulation software. Namballa [32] thinks that flow velocity and pressure could better describe the flow characteristics of CPB during pipeline transportation. CPB is laminar during pipeline transportation [33]. To address the research problem, minimize interference factors, and prevent model deformation, this study employed the laminar flow module using numerical simulation software to construct a 3D horizontal pipe model with a diameter of 200 mm and a length of 4 m. The model utilized a free-split tetrahedral mesh with 8 boundary layers and a stretch factor of 1.2. The simulated temperatures were 20 °C, 30 °C, 40 °C, and 50 °C. After verifying mesh independence, the final mesh count was determined to be 689,935, as illustrated in Figure 4.

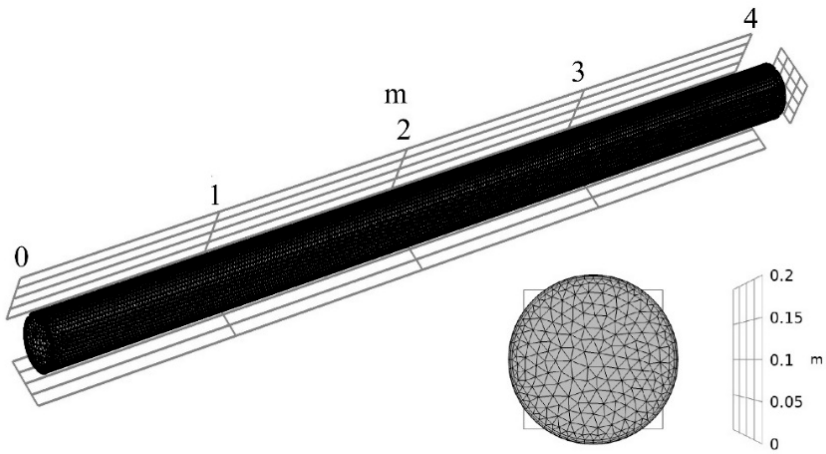


Figure 4. Mesh diagram of the pipeline section.

3. Results and Discussion

3.1. Rheological Test Results and Analysis

3.1.1. Shear Rate Ramp Loading Test Results and Analysis

As shown in Figure 5, with the increase in shear rate, the change in shear stress is mainly divided into two stages.

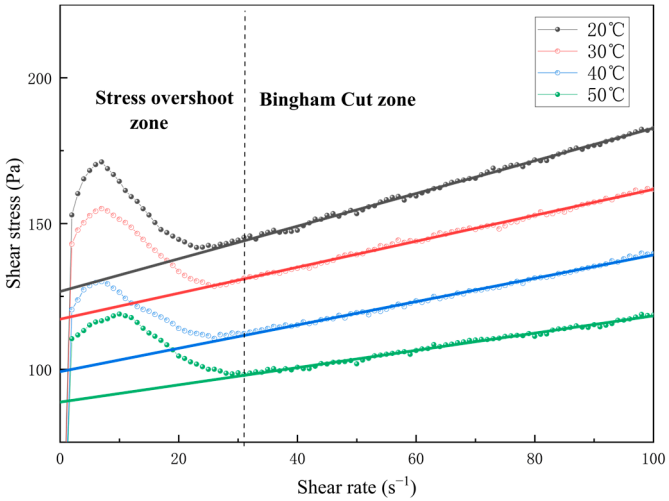


Figure 5. Rheological characteristic curve of CPB.

When strain is initially applied, the polymer molecular chains in the material lack sufficient time to relax or stretch, resulting in entanglement and friction among the chains. These entangled molecular chains produce a large resistance to deformation in a short period of time, causing the stresses to rise instantaneously and exceed the steady-state value, resulting in the phenomenon of "stress overshoot" [34]. The steady state of the slurry is subsequently disrupted, leading to the initiation of CPB flow. During the second stage, the stress overshoot progressively decreases, and the typical characteristics of CPB flow are observed.

Based on the test results, it is evident that the second stage of the rheological characteristic curve exhibits a linear increase, aligning with the characteristics of a Bingham plastic body. Consequently, the Bingham model represented by Equation (1) was employed for fitting, and the rheological parameters of CPB under different working conditions were obtained and are presented in Table 4.

$$\tau = \tau_0 + \eta\dot{\gamma} \quad (1)$$

Here, τ (Pa) is the shear stress, τ_0 (Pa) is the yield stress, η (Pa·s) is the plastic viscosity, and $\dot{\gamma}$ (s^{-1}) is the shear rate. It can be seen from Table 4 that with the increase in temperature, the molecular motion in CPB intensifies, the floc network structure in CPB is unstable, and the plastic viscosity and yield stress gradually decrease.

Table 4. Rheological parameters of CPB.

Sample ID	Temperature /°C	Plastic Viscosity /(Pa·s)	Yield Stress /Pa	R^2
R-20	20	0.85	128.355	0.99
R-30	30	0.77	117.7	0.99
R-40	40	0.69	99.28	0.99
R-50	50	0.62	88.78	0.99

3.1.2. Shear Rate Constant Loading Test Results and Analysis

The test results are shown in Figures 6–9. The stress relaxation curves of CPB under different conditions show similar variation laws. With the increase in shear time, the shear stress gradually decreases and then tends to be stable. The higher the shear rate, the higher the shear stress. The rheological parameters of CPB at different times can be obtained via regression analysis of the shear stress at multiple shear rates [33,35,36].

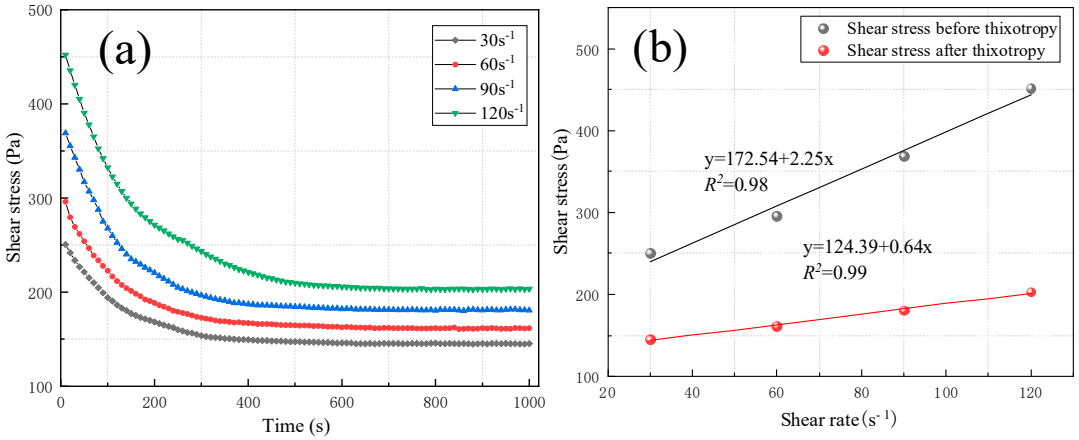


Figure 6. Test results of group C-20: (**a**) stress relaxation curve, (**b**) regression of rheological parameters before and after change.

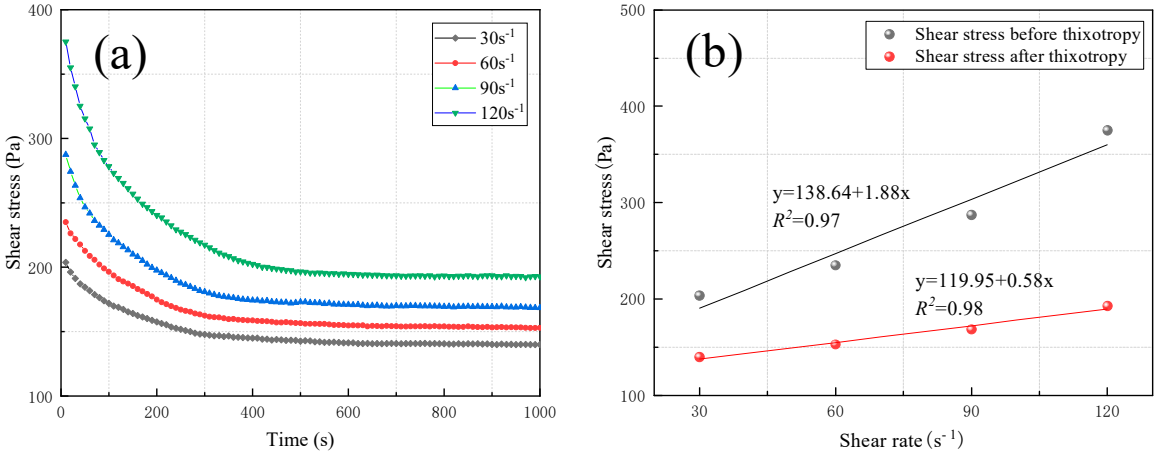


Figure 7. Test results of group C-30: (**a**) stress relaxation curve, (**b**) regression of rheological parameters before and after change.

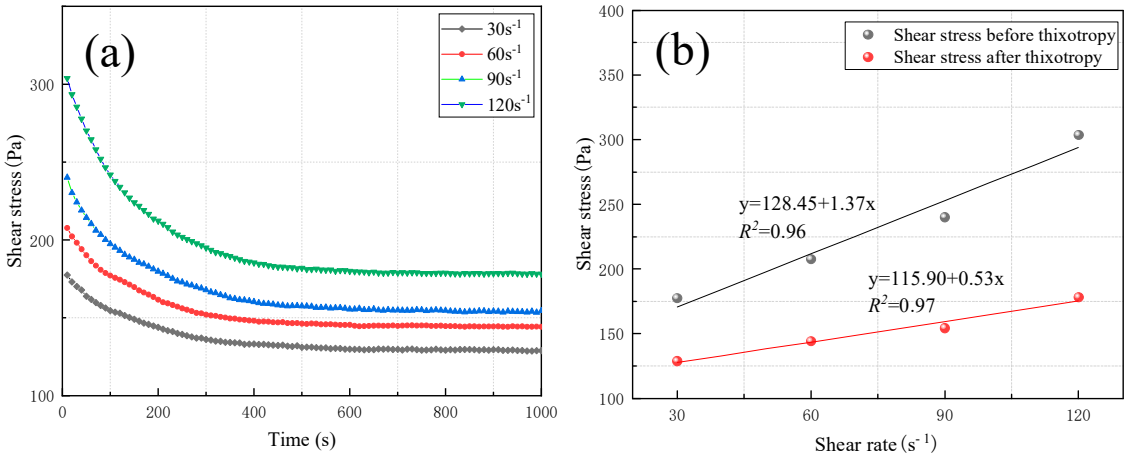


Figure 8. Test results of group C-40: (**a**) stress relaxation curve, (**b**) regression of rheological parameters before and after change.

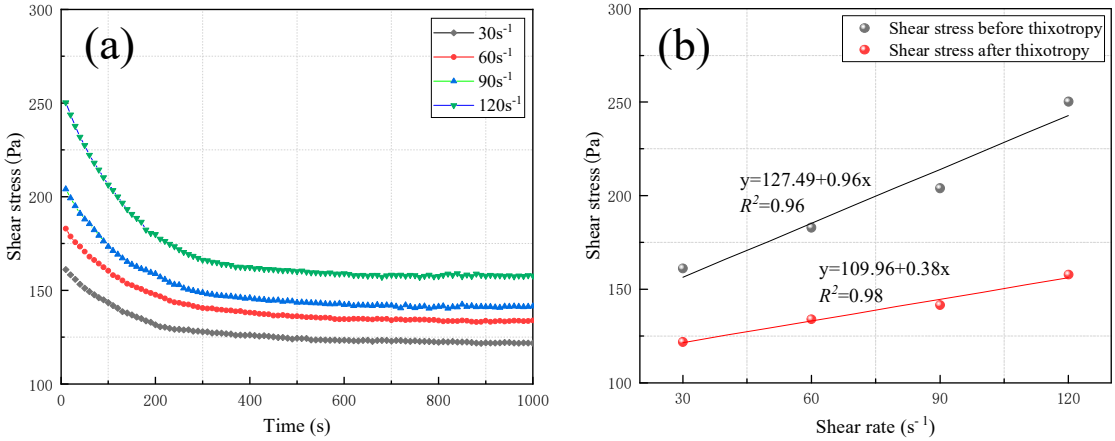


Figure 9. Test results of group C-50: (**a**) stress relaxation curve, (**b**) regression of rheological parameters before and after change.

By examining the stress relaxation curves of CPB under various shear rates, the shear stress values before and after change were determined. Subsequently, regression analysis

using the Bingham model was applied, demonstrating an excellent fitting degree. This indicates that the rheological properties of the transient CPB align with the characteristics of the Bingham fluid model.

3.2. Rheological Model for CPB Considering Time-Dependent Rheological Behavior

According to the stress relaxation curves of CPB under different shear rates obtained from the test, the yield stress and plastic viscosity can be obtained via regression analysis of the shear stress under multiple shear rates at each moment. To optimize the amount of data, regression analysis was performed every 100 s. The results are shown in Figure 10. As shown in Figure 10, both the plastic viscosity and the yield stress decrease gradually with the increase in shear time and finally level off.

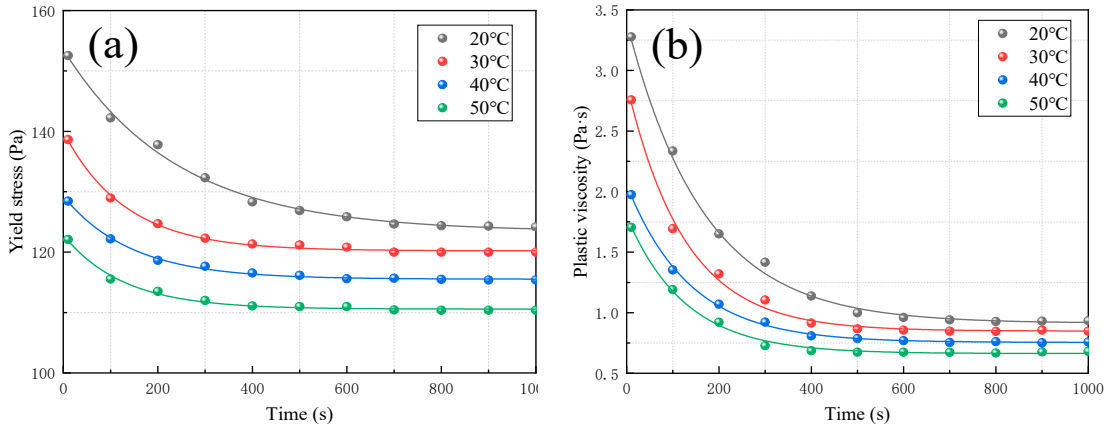


Figure 10. The rheological parameters of CPB varied with shear time at different temperatures: (**a**) yield stress variation law, (**b**) plastic viscosity change law.

Through observation, it can be found that the law of CPB yields stress changes with shear time that are similar at different temperatures. According to the change in yield stress with shear time, a composite function in the form of Equation (2) is constructed to characterize it.

$$\tau_0 = \tau_{eq} + \tau_{th} \cdot \exp^{-kt} \quad (2)$$

where τ_0 (Pa) is the yield stress, τ_{eq} (Pa) is the yield stress at equilibrium, τ_{th} (Pa) is the amount of time-dependent yield stress, k is the yield stress time-dependent parameters, and t (s) is shear time. Equation (2) was used to perform regression analysis on the yield stress time-dependent parameters of CPB, and the values of the parameters were obtained, as shown in Table 5.

Table 5. Yield stress time-dependent parameters regression analysis results.

Solid Content /%	Temperature /°C	τ_{eq}/Pa	τ_{th}/Pa	k	R^2
66	20	123.39	30.18	0.0042	0.98
	30	120.23	19.69	0.0066	0.99
	40	115.53	13.74	0.0070	0.99
	50	110.57	12.27	0.0080	0.98

The change law of the plastic viscosity of CPB at different temperatures is also similar. According to the change in plastic viscosity with time, a composite function of Equation (3) is constructed to characterize it.

$$\eta = \eta_{eq} + \eta_{th} \cdot \exp^{-st} \quad (3)$$

where η (Pa·s^{-1}) is the plastic viscosity, η_{eq} (Pa·s^{-1}) is the plastic viscosity at equilibrium, η_{th} (Pa·s^{-1}) is the time-dependent parameter of the plastic viscosity, s is the plastic viscosity time-dependent parameter, and t (s) is the shear time. Equation (3) was used to perform regression analysis on the plastic viscosity time-dependent parameters of CPB, and the values of the parameters were obtained, as shown in Table 6.

Table 6. Plastic viscosity time-dependent c parameter regression analysis results.

Solid Content /%	Temperature /°C	η_{eq}/Pa	η_{th}/Pa	s	R^2
66	20	0.91	2.48	0.0060	0.98
	30	0.84	2.04	0.0069	0.98
	40	0.75	1.30	0.0074	0.99
	50	0.66	1.13	0.0079	0.99

Through the correlation analysis, it can be found that the yield stress time-dependent parameter and the plastic viscosity time-dependent parameter of CPB have a strong correlation with temperature, as shown in Figure 11. τ_{eq}, η_{eq}, k, and s have an approximately linear relationship with temperature, while τ_{th} and η_{th} have a nonlinear relationship with temperature. The regression equation is shown in Table 7.

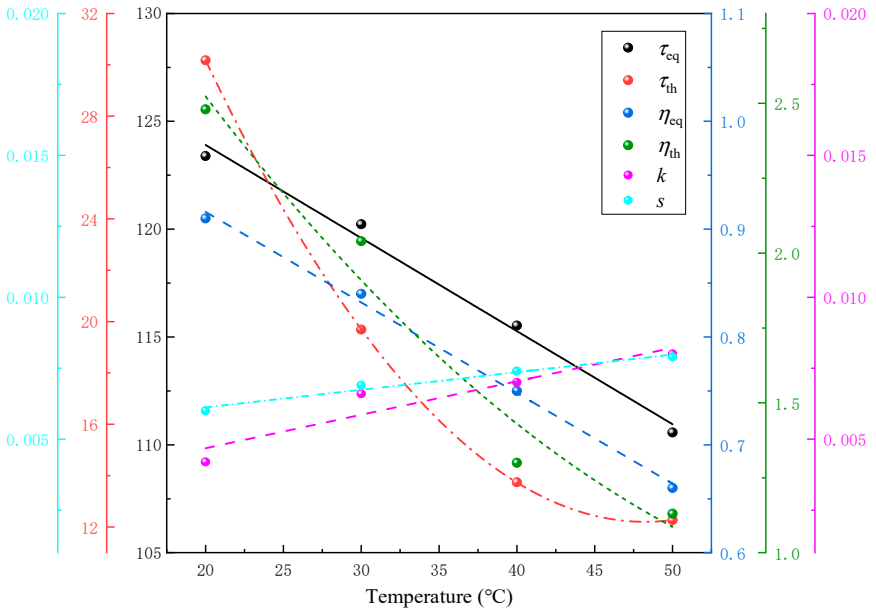


Figure 11. Time-dependent parameter regression curve.

Table 7. Time-dependent parameter regression results.

Time-Dependent Parameters	Fitting Equation	R^2
τ_{eq}	$\tau_{eq} = -0.43T + 132.54$	0.99
τ_{th}	$\tau_{th} = 0.023T^2 - 2.17T + 64.66$	0.99
η_{eq}	$\eta_{eq} = -0.0084T + 1.084$	0.99
η_{th}	$\eta_{th} = 0.00067T^2 - 0.095T + 4.15$	0.98
k	$k = 0.0023 + 1.18 \times 10^{-4}T$	0.95
s	$s = 0.0049 + 6.2 \times 10^{-5}T$	0.98

By substituting the time-dependent parameter regression equation into Equations (2) and (3), the rheological model considering temperature and time is obtained, as shown in Equations (4) and (5).

$$\tau_0 = 132.54 - 0.43T + (0.023T^2 - 2.17T + 64.66) \cdot \exp^{-(0.0023+1.18\times10^{-4}T)t} \quad (4)$$

$$\eta = 1.084 - 0.0084T + (0.00067T^2 - 0.095T + 4.15) \cdot \exp^{-(0.0049+6.2\times10^{-5}T)t} \quad (5)$$

The Bingham equation shows the relationship between rheological parameters and pipeline resistance. When the plastic viscosity and yield stress are known, Equation (6) can be used to calculate pipeline resistance [37–39].

$$i = \frac{\Delta P}{L} = \frac{16}{3D} \cdot \tau_0 + \frac{32v}{D^2} \cdot \eta \quad (6)$$

We next substitute Equations (4) and (5) into Equation (6) to obtain the calculation model of pipeline resistance considering temperature and time, as shown in Equation (7).

$$\begin{aligned} i = \tfrac{\Delta P}{L} = \tfrac{16}{3D} \cdot [132.54 - 0.43T + (0.023T^2 - 2.17T + 64.66) \cdot \exp^{-(0.0023+1.18\times10^{-4}T)t}] \\ + \tfrac{32v}{D^2} \cdot [1.084 - 0.0084T + (0.00067T^2 - 0.095T + 4.15) \cdot \exp^{-(0.0049+6.2\times10^{-5}T)t}] \end{aligned} \quad (7)$$

3.3. Validation

The actual pipeline conveying resistance was monitored at a mine site, where the CPB concentration was 66%~68%, the inner diameter of the filling pipeline was 175 mm, and the filling flow rate was 130~150 m^3/h. The measured actual pressure loss at different conveying distances (transport time) and the calculated pressure loss in the model are shown in Figure 12. Due to the wall slip effect, there is a certain error between the calculated value and the actual value, but the error is small, and the model calculation is more accurate.

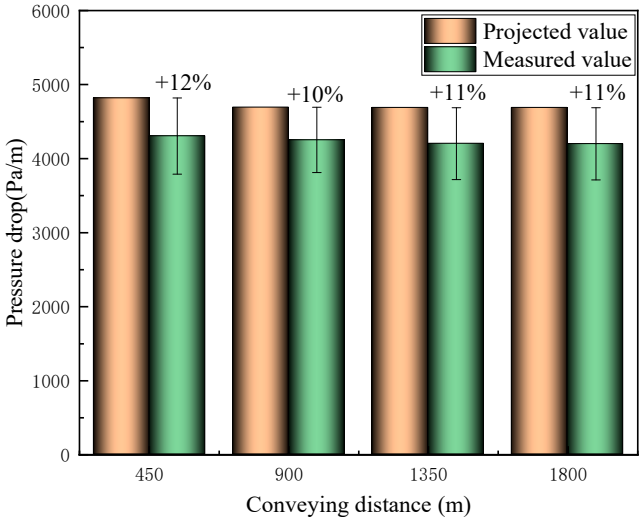


Figure 12. Validation of numerical simulation model.

4. Numerical Simulation Considering Time and Temperature

4.1. Model Assumption

For the convenience of analysis, this study makes the following assumptions about the flow of CPB in the pipe based on the theory of fluid mechanics:

(1) The fluid in the pipe is homogeneous.
(2) The filling slurry is regarded as an incompressible fluid.
(3) The flow of CPB in the pipe is gapless, i.e., the flow is continuous.

4.2. Control Equations

The fundamental equation describing fluid flow in numerical simulation software is the Navier–Stokes (N-S) equation, as shown in Equation (8). In order to accommodate different simulated materials, a weakly solved form of Equation (7) is substituted into the governing equations to create a numerical model that takes into account both temperature and time:

$$\begin{cases} \rho\frac{\partial u}{\partial t} + \rho(u \cdot \nabla)u = \nabla \cdot \left\{u\left[\nabla u + (\nabla u)^T\right] - pl - \frac{2}{3}\mu(\nabla \cdot u)l\right\} + F \\ \frac{\partial u}{\partial t} + \nabla(u \cdot \rho) = 0 \\ \rho = (p, T) \end{cases} \quad (8)$$

where u (m/s) is the velocity, ρ (kg/m^3) is the intensity, p (Pa) is stresses, l is the unit tensor, and F (N) is the volumetric force.

4.3. Boundary Conditions

In pipeline transportation, it is generally considered that the pipeline inlet is a uniform flow, so the inlet is set as the normal flow velocity inlet, the flow state is laminar, and the flow rate of CPB in the actual pipeline conveying process is generally 1~2 m/s, taking the average value of 1.5 m/s as the inlet flow rate. Wall slip is not considered. Because gravity is set as the body force, if the outlet condition is set to zero, the calculation results will not converge, or the results will be wrong. Therefore, it is necessary to set the outlet to an outlet with an open boundary and no viscous stress and add constraint conditions.

4.4. Pipe Flow Properties of CPB

4.4.1. Velocity Distribution of CPB Pipeline Transportation

To investigate the velocity distribution along the axial direction, the velocity profile of the CPB pipeline was sliced (Figure 13). As depicted in Figure 13, upon entering the pipeline, the CPB exhibits plunger flow in the central area, while the side wall area experiences shear flow due to elevated frictional resistance against the pipe wall.

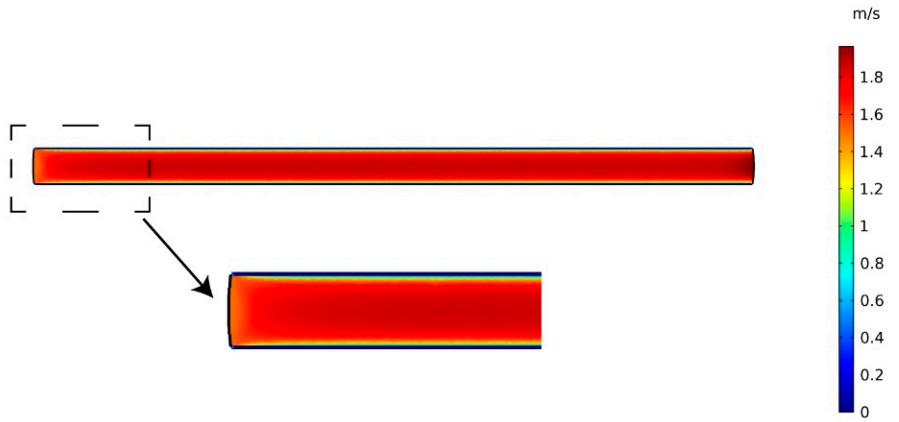


Figure 13. CPB flow velocity axial slice.

The velocity vector was proportionally deformed to illustrate the velocity distribution along the pipeline. As depicted in Figure 14, as the transport distance increases, the velocity difference between the plunger flow area and the shear flow area gradually expands. This is because, in the shear flow region, the velocity of the slurry is gradually reduced by the shear effect, while the plunger flow region has less shear effect, which leads to a gradual increase in the velocity difference. The shearing action continuously disrupts the structure of the CPB at the edge of the plug flow area, leading to a gradual reduction in the plug flow area and an increase in the shear flow area.

To examine the impact of temperature on the flow velocity of CPB, data on vertical flow velocity distribution at 2 m of the pipeline were extracted at different temperatures using

the "defined cutting line" method for comparative analysis. As illustrated in Figure 15, the flow patterns of CPB at different temperatures exhibit similarities.

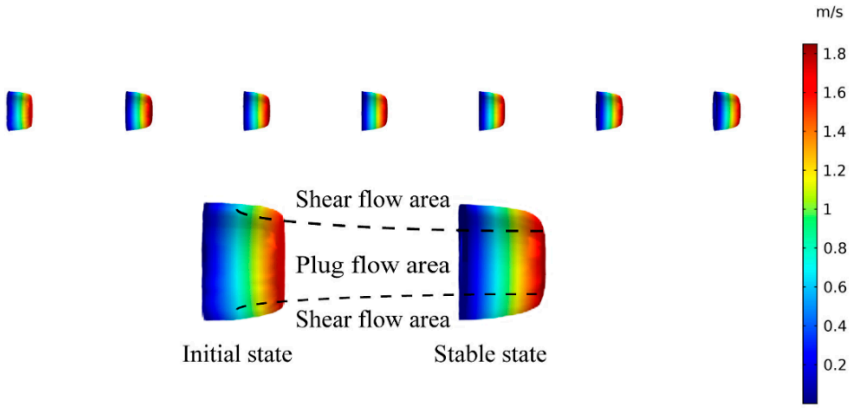


Figure 14. CPB flow velocity vector map.

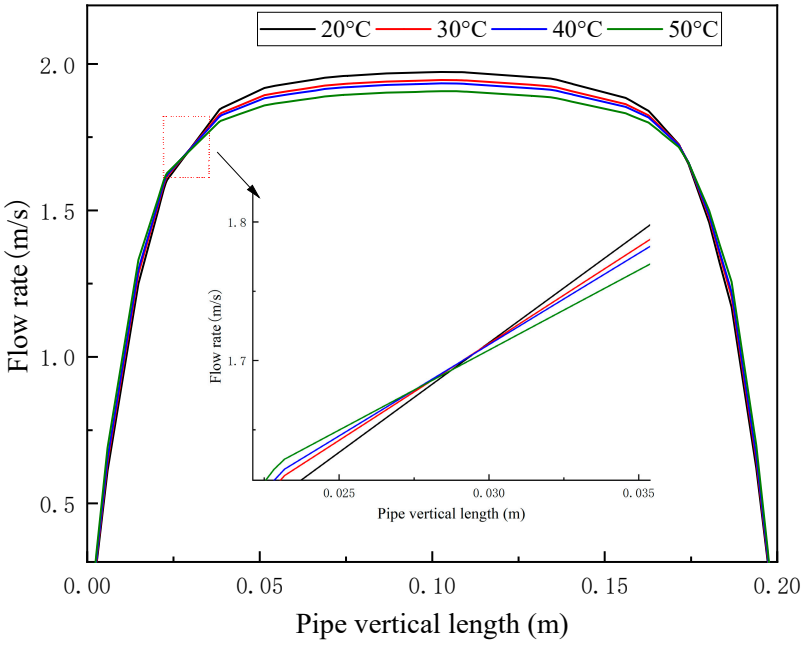


Figure 15. Flow velocity distribution at 2 m of pipeline at different temperatures.

In the plunger flow area, higher temperatures result in reduced rheological parameters, leading to an overall unstable structure. The acceleration under shear effects decreases, causing a smaller flow velocity. In the shear flow area, higher temperatures lead to smaller rheological parameters, resulting in reduced flow resistance and increased flow velocity.

4.4.2. CPB Pipeline Transportation Resistance at Different Temperatures

As depicted in Figure 16, an increase in temperature correlates with a gradual decrease in pipeline transportation resistance. Through analysis, it is observed that the temperature rise enhances the Brownian motion of molecules in CPB, liberating it from the constraints of van der Waals forces. The CPB undergoes a transition from a floc network structure to a liquid network structure, resulting in more free water. This ultimately results in a decrease in rheological parameters, effectively reducing pipeline transportation resistance.

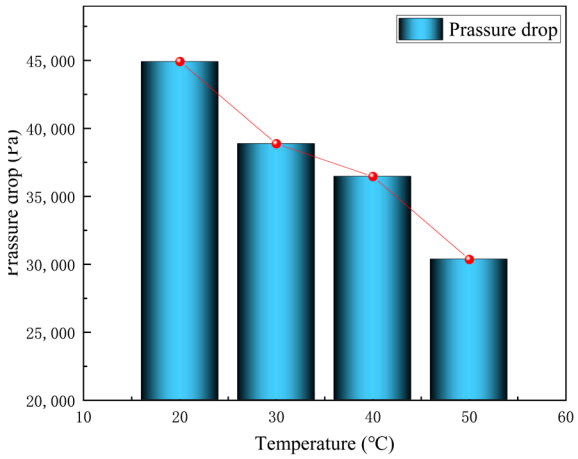


Figure 16. Influence of temperature on pipeline transportation resistance.

4.5. Time-Dependent Rheological Behavior of CPB

As illustrated in Figures 17 and 18, the plastic viscosity and yield stress of CPB exhibit a gradual decrease with an increase in transport distance. In the central area of the pipeline, where CPB demonstrates plug flow with less shear, the plastic viscosity and yield stress are relatively high. On the other hand, in the side wall area of the pipeline, the floc network structure of CPB undergoes damage due to shearing, resulting in lower plastic viscosity and yield stress.

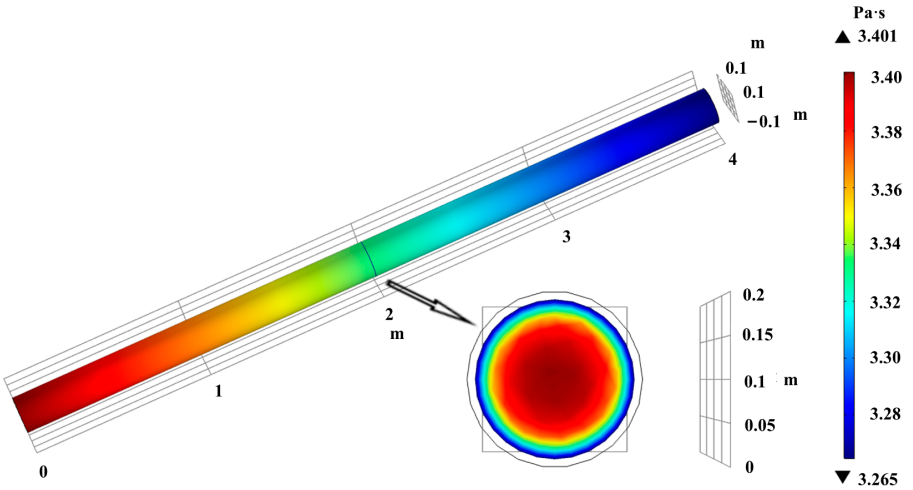


Figure 17. Plastic viscosity distribution.

As depicted in Figure 19, temperature exerts a noticeable influence on the time-dependent rheological behavior of CPB. In the same duration, the time-dependent rheological behavior of CPB varies at different temperatures. Time-dependent rheological behavior is discerned by changes in plastic viscosity and yield stress; notably, higher temperatures correspond to smaller variations in plastic viscosity and yield stress.

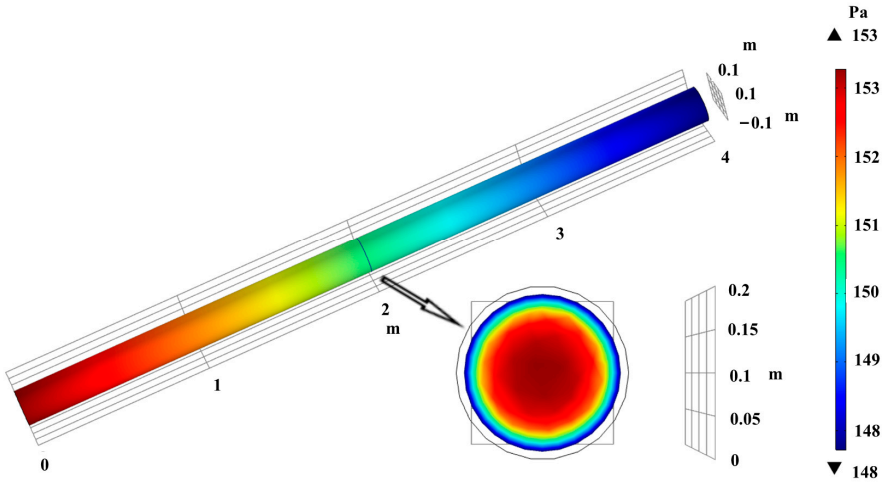


Figure 18. Yield stress distribution.

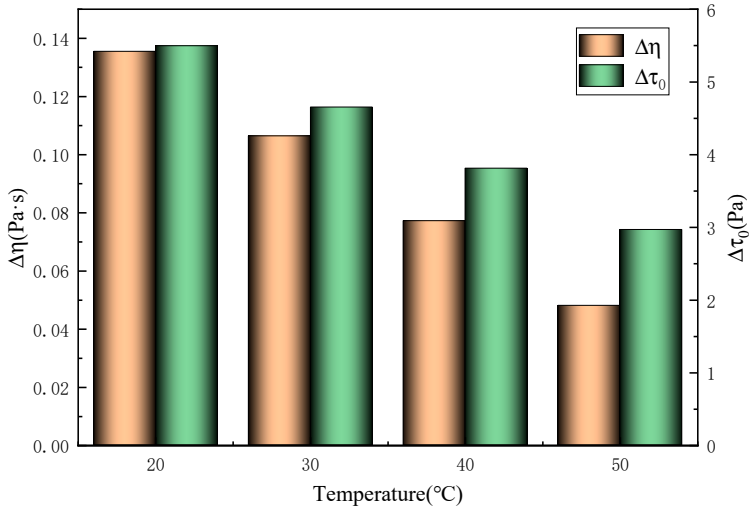


Figure 19. The effects of temperature on the time-dependent rheological behavior of CPB.

5. Conclusions

The effects of temperature on the time-dependent rheological behavior of CPB were analyzed through experiments and numerical simulations. The following conclusions were drawn:

1. CPB, as a non-Newtonian fluid, exhibits changes in its rheological properties influenced by both time and temperature. Traditional models overlook the time-dependent characteristics, whereas we have formulated a coupled model that incorporates the influences of temperature and time based on rheological experimental results.
2. We embedded a coupled model considering temperature and time in numerical simulation software to achieve the three-dimensional visualization of the CPB pipeline transportation process. The findings revealed that CPB exhibits plug flow during pipeline transportation. In the plug flow zone, higher temperatures correspond to a reduced flow rate, whereas in the shear flow zone, the opposite holds true. Additionally, the pipeline resistance of CPB decreases with the increase in temperature.
3. Temperature affects the time-dependent rheological behavior of CPB. Within the range of 20 °C~50 °C, it was observed that the higher the temperature, the less the rheology of CPB was affected by shear time. At the same shear time, the changes in plastic viscosity and yield stress were 1.6 Pa·s and 48.15 Pa, respectively, at 20 °C. When the temperature increased to 50 °C, the change in plastic viscosity was reduced to 0.58 Pa·s, and the change in yield stress was reduced to 12.53 Pa.

In future research, there is a need to establish a more realistic numerical simulation that incorporates a multi-field coupling mechanism, accounting for various influencing factors. This approach aims to provide a more accurate representation of the flow process within the CPB pipeline. For instance, it should consider the particle migration and pipeline wear mechanisms of CPB during transportation under the influence of multi-field coupling.

Author Contributions: B.L.: data curation, writing—original draft, methodology. Y.Z.: writing—review and editing. X.Z.: conceptualization, methodology. C.Z.: data curation, writing—review and editing, methodology. Y.C.: software, formal analysis. All authors have read and agreed to the published version of the manuscript.

Funding: This research was funded by Bo Liu grant number GJJ2403710. And the APC was funded by Bo Liu.

Data Availability Statement: The raw data supporting the conclusions of this article will be made available by the authors on request.

Acknowledgments: This work was supported by the Foundation of Jiangxi Educational Committee (GJJ2403710).

Conflicts of Interest: The authors declare that they have no known competing financial interests or personal relationships that could have appeared to influence the work reported in this paper.

References

1. Orejarena, L.; Fall, M. The use of artificial neural networks to predict the effect of sulphate attack on the strength of cemented paste backfill. *Bull. Eng. Geol. Environ.* **2010**, *69*, 659–670. [CrossRef]
2. Qi, C.C.; Ly, H.B.; Le, L.M.; Yang, X.Y.; Guo, L.; Pham, B.T. Improved strength prediction of cemented paste backfill using a novel model based on adaptive neuro fuzzy inference system and artificial bee colony. *Constr. Build. Mater.* **2021**, *284*, 122857. [CrossRef]
3. Fall, M.; Benzaazoua, M. Modeling the effect of sulphate on strength development of paste backfill and binder mixture optimization. *Cem. Concr. Res.* **2005**, *35*, 301–314. [CrossRef]
4. Jafari, M.; Shahsavari, M.; Grabinsky, M. Experimental Study of the Behavior of Cemented Paste Backfill under High Isotropic Compression. *J. Geotech. Geoenviron. Eng.* **2020**, *146*, 06020019. [CrossRef]
5. Tana, A.E.B.; Yin, S.H.; Wang, L.M. Investigation on Mechanical Characteristics and Microstructure of Cemented Whole Tailings Backfill. *Minerals* **2021**, *11*, 592. [CrossRef]
6. Wu, A.X.; Ruan, Z.E.; Wang, J.D. Rheological behavior of paste in metal mines. *Int. J. Miner. Metall. Mater.* **2022**, *29*, 717–726. [CrossRef]
7. Liu, L.; Ruan, S.S.; Qi, C.C.; Zhang, B.; Tu, B.B.; Yang, Q.X.; Song, K. Co-disposal of magnesium slag and high-calcium fly ash as cementitious materials in backfill. *J. Clean. Prod.* **2021**, *279*, 123684. [CrossRef]
8. Chen, Q.S.; Tao, Y.B.; Zhang, Q.L.; Qi, C.C. The rheological, mechanical and heavy metal leaching properties of cemented paste backfill under the influence of anionic polyacrylamide. *Chemosphere* **2022**, *286*, 131630. [CrossRef]
9. Xue, Z.L.; Gan, D.Q.; Zhang, Y.Z.; Liu, Z.Y. Rheological behavior of ultrafine-tailings cemented paste backfill in high-temperature mining conditions. *Constr. Build. Mater.* **2020**, *253*, 119212. [CrossRef]
10. Yan, Z.P.; Yin, S.H.; Chen, X.; Wang, L.M. Rheological properties and wall-slip behavior of cemented tailing-waste rock backfill (CTWB) paste. *Constr. Build. Mater.* **2022**, *324*, 126723. [CrossRef]
11. Gao, R.G.; Zhou, K.P.; Zhou, Y.L.; Yang, C. Research on the fluid characteristics of cemented backfill pipeline transportation of mineral processing tailings. *Alex. Eng. J.* **2020**, *59*, 4409–4426. [CrossRef]
12. Jiang, H.Q.; Qi, Z.J.; Yilmaz, E.; Han, J.; Qiu, J.P.; Dong, C.L. Effectiveness of alkali-activated slag as alternative binder on workability and early age compressive strength of cemented paste backfills. *Constr. Build. Mater.* **2019**, *218*, 689–700. [CrossRef]
13. Zhao, Y.; Taheri, A.; Karakus, M.; Chen, Z.W.; Deng, A. Effects of water content, water type and temperature on the rheological behavior of slag-cement and fly ash-cement paste backfill. *Int. J. Min. Sci. Technol.* **2020**, *30*, 271–278. [CrossRef]
14. Haruna, S.; Fall, M. Time- and temperature-dependent rheological properties of cemented paste backfill that contains superplasticizer. *Powder Technol.* **2020**, *360*, 731–740. [CrossRef]
15. Cao, S.; Yilmaz, E.; Song, W.D. Evaluation of Viscosity, Strength and Microstructural Properties of Cemented Tailings Backfill, Minerals. *Minerals* **2018**, *8*, 352. [CrossRef]
16. Xu, W.B.; Tian, M.M.; Li, Q.L. Time-dependent rheological properties and mechanical performance of fresh cemented tailings backfill containing flocculants. *Miner. Eng.* **2020**, *145*, 106064. [CrossRef]
17. Xu, W.B.; Zhang, Y.L.; Zuo, X.H.; Hong, M. Time-dependent rheological and mechanical properties of silica fume modified cemented tailings backfill in low temperature environment. *Cem. Concr. Compos.* **2020**, *114*, 103804. [CrossRef]
18. Zhou, Z.B.; Liu, J.H.; Zhou, Q.; Wu, A.X.; Wang, H.J. A New High Charge Density Superplasticizer Regulates the Rheological Properties of Tailings Slurry and Cemented Paste Backfill Materials. *Min. Metall. Explor.* **2022**, *39*, 749–759.

19. Deng, X.J.; Klein, B.; Zhang, J.X.; Hallbom, D.; de Wit, B. Time-dependent rheological behavior of cemented backfill mixture. *Int. J. Min. Reclam. Environ.* **2018**, *32*, 145–162. [CrossRef]
20. Mendes, P.R.D.S.; Abedi, B.; Thompson, R.L. Constructing a thixotropy model from rheological experiments. *J. Non-Newton. Fluid Mech.* **2018**, *261*, 1–8. [CrossRef]
21. Ali, G.; Fall, M.; Alainachi, I. Time- and Temperature-Dependence of Rheological Properties of Cemented Tailings Backfill with Sodium Silicate. *J. Mater. Civ. Eng.* **2021**, *33*, 04020498. [CrossRef]
22. Wang, X.M.; Li, J.X.; Xiao, Z.Z.; Xiao, W.G. Rheological properties of tailing paste slurry. *J. Cent. South Univ. Technol.* **2004**, *11*, 75–79. [CrossRef]
23. Wang, J.D.; Wu, A.X.; Ruan, Z.E.; Burger, R.; Wang, Y.M.; Wang, S.Y.; Zhang, P.F.; Gao, Z.Q. Optimization of Parameters for Rheological Properties and Strength of Cemented Paste Backfill Blended with Coarse Aggregates. *Minerals* **2022**, *12*, 374. [CrossRef]
24. Wu, D.; Cai, S.J.; Huang, G. Coupled effect of cement hydration and temperature on rheological properties of fresh cemented tailings backfill slurry. *Trans. Nonferrous Met. Soc. China* **2014**, *24*, 2954–2963. [CrossRef]
25. Lang, L.; Song, K.I.; Lao, D.Z.; Kwon, T.H. Rheological Properties of Cemented Tailing Backfill and the Construction of a Prediction Model. *Materials* **2015**, *8*, 2076–2092. [CrossRef]
26. Mewis, J.; Wagner, N.J. Thixotropy. *Adv. Colloid Interface Sci.* **2009**, *147*, 214–227. [CrossRef]
27. Liu, K.Q.; Yang, Y.; Zhang, X.N.; Zhu, K.L.; Wang, J.S.; Li, L.K.; Tu, Q.; Ma, R.R.; Cheng, X.W.; Zhang, X.G. Time-varying characteristics and mechanisms of hydrostatic pressure descent of Portland cement slurry. *Powder Technol.* **2021**, *385*, 434–443. [CrossRef]
28. Mendes, P.R.D.S. Modeling the thixotropic behavior of structured fluids. *J. Non-Newton. Fluid Mech.* **2009**, *164*, 66–75. [CrossRef]
29. Kaushal, D.R.; Thinglas, T.; Tomita, Y.; Kuchii, S.; Tsukamoto, H. CFD modeling for pipeline flow of fine particles at high concentration. *Int. J. Multiph. Flow* **2012**, *43*, 85–100. [CrossRef]
30. Liu, L.; Fang, Z.Y.; Qi, C.C.; Zhang, B.; Guo, L.J.; Song, K. Numerical study on the pipe flow characteristics of the cemented paste backfill slurry considering hydration effects. *Powder Technol.* **2019**, *343*, 454–464. [CrossRef]
31. Yin, S.H.; Shao, Y.J.; Wu, A.X.; Wang, H.J.; Liu, X.H.; Wang, Y. A systematic review of paste technology in metal mines for cleaner production in China. *J. Clean. Prod.* **2020**, *247*, 119590. [CrossRef]
32. Rao, N.D.; Thatoi, D.N.; Biswal, S.K. Rheological study and numerical analysis of high concentration iron ore slurry pipeline transportation. *Mater. Today Proc.* **2020**, *22*, 3197–3202.
33. Cheng, H.Y.; Wu, S.C.; Li, H.; Zhang, X.Q. Influence of time and temperature on rheology and flow performance of cemented paste backfill. *Constr. Build. Mater.* **2020**, *231*, 117117. [CrossRef]
34. Al-Zahrani, S.M. A generalized rheological model for shear thinning fluids. *J. Pet. Sci. Eng.* **1997**, *17*, 211–215. [CrossRef]
35. Qian, Y.; Kawashima, S. Use of creep recovery protocol to measure static yield stress and structural rebuilding of fresh cement pastes. *Cem. Concr. Res.* **2016**, *90*, 73–79. [CrossRef]
36. Huang, D.M.; Xing, D.Q.; Chang, X.K.; Zhu, Y.Y.; Gao, C.J. Analysis and Application of Filling Mining Technology in China's Mining Area: A Case Study of Yuxing Coal Mine. *Arch. Min. Sci.* **2021**, *66*, 611–624.
37. Li, M.Z.; He, Y.P.; Liu, Y.D.; Huang, C. Effect of interaction of particles with different sizes on particle kinetics in multi-sized slurry transport by pipeline. *Powder Technol.* **2018**, *338*, 915–930. [CrossRef]
38. Liu, Z.Y.; Gan, D.Q.; Gan, Z. Dynamic regimes of cemented backfill at early-age. *J. Cent. South Univ.* **2021**, *28*, 2079–2090. [CrossRef]
39. He, M.Z.; Wang, Y.M.; Forssberg, E. Slurry rheology in wet ultrafine grinding of industrial minerals: A review. *Powder Technol.* **2004**, *147*, 94–112. [CrossRef]

Disclaimer/Publisher's Note: The statements, opinions and data contained in all publications are solely those of the individual author(s) and contributor(s) and not of MDPI and/or the editor(s). MDPI and/or the editor(s) disclaim responsibility for any injury to people or property resulting from any ideas, methods, instructions or products referred to in the content.